Received 3 May 2024; accepted 9 June 2024. Date of publication 12 June 2024; date of current version 24 September 2024.

Digital Object Identifier 10.1109/OJAP.2024.3413020

A Single Radiator-Based Circularly Polarized Antenna for Indoor Wireless Communication Applications

HENG-TUNG HSU [1] (Senior Member, IEEE), YI-FAN TSAO [2] (Member, IEEE), AND ARPAN DESAI [3] (Senior Member, IEEE)

[1]International College of Semiconductor Technology, National Yang Ming Chiao Tung University, Hsinchu 300, Taiwan

[2]Industry Academia Innovation School, Institute of Pioneer Semiconductor Innovation, National Yang Ming Chiao Tung University, Hsinchu 300, Taiwan

[3]Department of Information and Communication Technology, Pandit Deendayal Energy University, Gandhinagar 382009, India

CORRESPONDING AUTHOR: A. DESAI (e-mail: arpan.desai@sot.pdpu.ac.in)

This work was supported in part by the National Science and Technology Council, Taiwan, under Grant NSTC 112-2221-E-A49-170-MY2, Grant NSTC 112-2622-8-A49-013-SB, Grant NSTC 112-2622-8-002-020, Grant NSTC 113-2218-E-A49-020, Grant NSTC 113-2927-I-A49-506, and Grant NSTC 113-2634-F-A49-008; and in part by the National Science and Technology Council, Taiwan, T-Star Center Project "Future Semiconductor Technology Research Center."

ABSTRACT This paper introduces a novel technique for inducing circular polarization in a single radiator through the implementation of a sequentially rotated feeding network. Analogous to the operational principles of sequentially rotated antennas employing multiple radiators, the creation of circular polarization (CP) with a solitary radiator becomes achievable through the distinctive phase and angular arrangement facilitated by the feeding network. This innovative approach not only results in a substantial reduction in complexity but also contributes to an overall reduction in antenna size, all while upholding commendable CP performance in terms of both axial ratio (AR) bandwidth and beamwidth.

INDEX TERMS Axial ratio (AR), AR bandwidth, AR beam width, circular polarization, sequential rotation.

I. INTRODUCTION

THE rapid evolution of wireless communication systems necessitates circularly polarized (CP) antennas that facilitate communication between transmitters and receivers with less stringent requirements regarding polarization orientation. In comparison to linearly polarized antennas, CP antennas exhibit lower sensitivity to multipath fading and interference [1], [2]. Antennas with wide axial ratio (AR) bandwidth, impedance bandwidth, directional radiation patterns, and high gain are crucial for maintaining overall system performance.

CP antennas can be implemented in single-layer or multilayer configurations, with the former being popular due to its compact size. Achieving CP characteristics in a single-layer configuration involves employing a single patch radiator with truncated corners, multiple feeds featuring proper phase offsets, and circular-shaped geometries. While enhancing AR performance is feasible with multiple radiators arranged in an array configuration, this approach falls short of achieving a satisfactory AR bandwidth, particularly when designed with thin dielectric substrates [3]. Furthermore, the impedance bandwidth is limited due to the high-quality factor (Q) nature of thin substrates [4], resulting in limited gain and less directive radiation patterns.

In contrast, multi-layer structures have demonstrated substantial performance improvements. A comprehensive study [5] indicated a significant enhancement in AR bandwidth from 0.8% to 4.6%. Alternative approaches, such as incorporating circular parasitic patches as directors [6], have also proven effective for improving AR bandwidth.

The challenge of achieving an even wider AR bandwidth, exceeding 10%, using a single radiator has been addressed in [7]. The proposed technique involves sequentially rotating individual radiators with a unique phase offset,

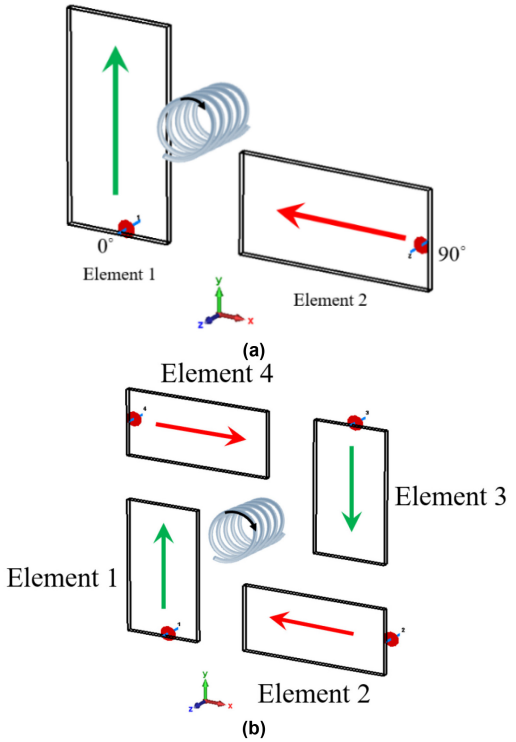

FIGURE 1. The mechanism for CP generation: (a) using two mutually orthogonal elements with proper phase offset, (b) using two pairs of (a) with 90o phase offset for the improvement of AR bandwidth and beam width.

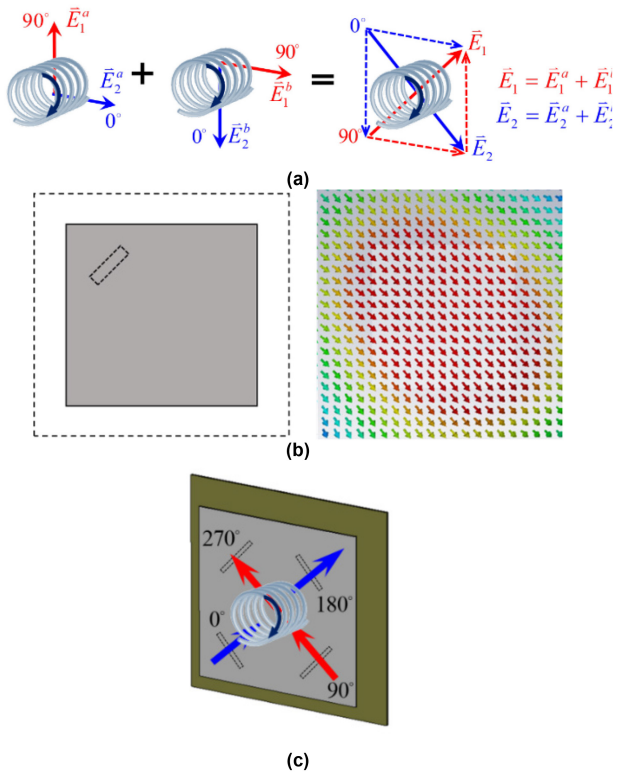

FIGURE 2. The illustration of the mechanism generating CP performance using a single radiator with a sequentially rotated feeding network: (a) the basic building blocks showing the composition of two mutually-orthogonal pairs of E-field components; (b) simulation verification of the aperture-coupled square patch radiator to generate the required E-field components and (c) final configuration of the proposed antenna featuring single radiator.

leading to a substantial improvement in AR bandwidth. Additionally, the AR beamwidth is enhanced due to the cancellation of cross-polarization fields and reinforcement of co-polarization fields attributed to the assigned phase offset [7].

The fundamental mechanism for CP generation using linearly polarized elements involves two mutually orthogonal radiation field components with a 90-degree offset at the feeds, as illustrated in Fig. 1(a) [7]. The drawback of this configuration is poor AR beamwidth due to extra spatial phase delays caused by offset in the broadside direction. To address this issue, two more elements are added, as depicted in Fig. 1(b), resulting in improved AR bandwidth and beamwidth [7]. The sequentially-rotated radiator approach, while offering significant improvements, suffers from increased size due to the number of radiators. The primary objective of the proposed antenna is to realize circular polarization using a single radiator in an aperture-coupled configuration. Four slots are utilized that are placed perpendicularly to each other, and feed through 90° phase shifted signals, which couple the EM energy to the top conducting patch. As observed in Fig. 2(a), it is depicted that two perpendicularly polarized fields generated from the two orthogonally placed linearly polarized elements and provided with the necessary phase shifts will lead to the generation of circular polarization. As discussed previously, using only two elements will lead to extra spatial phase delays, leading to poor AR due to higher cross-pol levels. So, in this case, 2, more elements are utilized for good cross-pol cancellation, leading to a better axial ratio. In the proposed antenna, the slots are arranged diagonally, and the electric field due to a single slot is illustrated in Fig. 2(b). Fig. 2(c) shows the final configuration using 4 slots placed diagonally in an orthogonal manner. The sequential feeding network featuring a progressive 90° phase difference is used to excite the slots and eventually coupling of EM energy to the top patch. Specifically, the ports feeding the four coupling slots have phases of 0°, 90°, 180°, and 270° with nearly equal amplitudes. This paper proposes a technique to achieve the same CP characteristics with a single radiator. The configuration involves the physical rotation of coupling slots sequentially with the same phase offset, enhancing the AR bandwidth and beamwidth similar to the sequentially-rotated radiators configuration [7]. The key advantage of this proposed configuration is its compact size, as only one radiator is involved in CP generation. To validate the technique, an antenna for radio-frequency identification (RFID) reader applications is proposed. RFID systems necessitate antennas with excellent CP performance to establish communication links between readers and tags in a complex environment. Based on the proposed sequentially-rotated feeding architecture, an aperture-coupled patch antenna was realized, covering an impedance bandwidth of S11 less

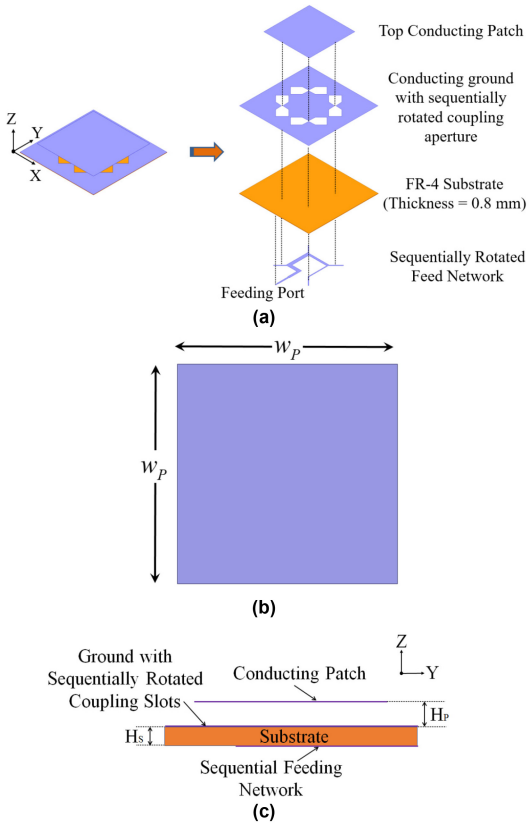

FIGURE 3. Proposed antenna geometry: (a) layered view; (b) top patch; (c) side view.

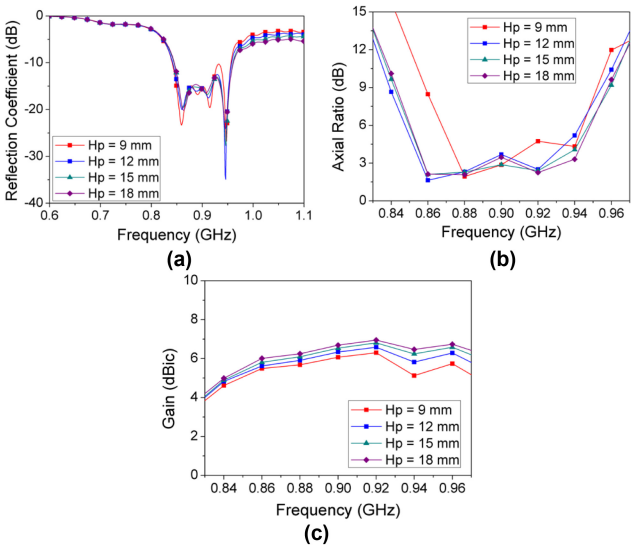

FIGURE 4. The effect of Hp on (a) S11, (b) AR, and (c) gain versus frequency.

than -10 dB from 845-964 MHz. The antenna exhibited left-hand circularly-polarized (LHCP) radiation characteristics with a gain of 7.8 dBic, an AR bandwidth (AR<3 dB) of 67 MHz (865-932 MHz), and an AR beamwidth of 105° at the center frequency. The reader antenna's read range is 2.7 meters and 4 meters at EIRP of 2.1 W and 4 W, respectively.

II. ANTENNA GEOMETRY

The design of the antenna with circular polarization relies on exciting orthogonal modes with a 90° phase shift and equal magnitude. In this section, we introduce the geometry of an aperture-coupled multilayer circularly polarized antenna fed by a single sequentially-rotated feed. The proposed multilayer antenna configuration using a single radiator is depicted in Fig. 3. The antenna comprises two main components: a bottom printed circuit board (PCB) and a single radiator separated by an air gap. The bottom PCB features a sequentially rotated feeding network with the desired phase offset on the bottom layer and rotated slots inclined at an angle of 45° on the top side of the board. The PCB used is the FR-4 substrate with a height, relative permittivity, and loss tangent of 0.8 mm, 4.34, and 0.025, respectively. Fig. 3 displays the layered view, top patch, and side view of the antenna.

Fig. 3(a) illustrates that the antenna consists of four layers, including one substrate and three metal layers. The antenna is excited by the sequentially rotated feeding network, coupling electromagnetic radiation to the top square radiator through sequentially rotated inclined slots etched on the ground plane. Such an aperture-coupled patch configuration generally exhibits a reasonable impedance bandwidth, as well as directive radiation patterns. The enhanced bandwidth of an aperture-coupled patch setup stems from increased design flexibility afforded by tuning stub length and coupling aperture size. These elements allow precise adjustment to counteract impedance shifts and optimize resonance, yielding a double-tuning effect. Additionally, stacked patch configurations provide further tuning capabilities, boosting bandwidth and performance. Furthermore, aperture-coupled designs enable precise control over radiation characteristics, yielding directive radiation patterns. By manipulating the dimensions of the aperture, patch, and coupling mechanism, designers can tailor patterns for specific needs like beam steering or shaping.

The top conducting patch is depicted in Fig. 3(b), positioned 15 mm away from the ground plane, as visible in Fig. 3(c). A parametric study to investigate the effect of H_p on the antenna performance is carried out. Fig. 4 (a-c) shows the results of such analysis in terms of S11, AR, and gain versus frequency. As observed, the spacing H_p does not have much effect on the S11 and gain performance yet AR is more dependent on H_p. Based on the simulation results, the value of H_p as 15 mm is selected for practical realization.

The four slots etched on the ground plane are depicted in Fig. 5(a), inclined at an angle of ±45° and sequentially rotated by 90° relative to the adjacent ones. The hourglass-shaped slot is chosen for its contribution to maximum coupling with minimal back radiation. The hourglass-shaped slot in an aperture-coupled patch antenna optimizes coupling while minimizing back radiation through several key mechanisms. Its unique form efficiently channels electromagnetic

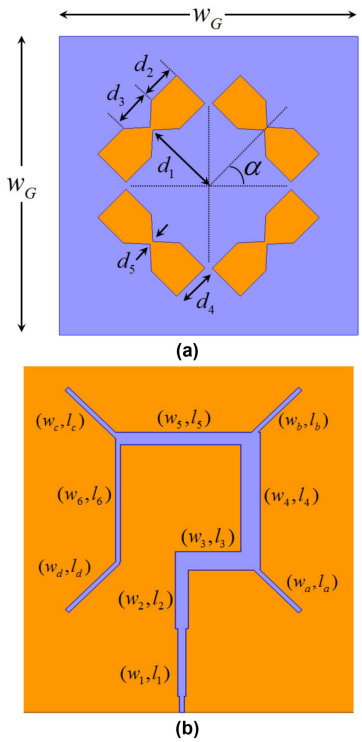

FIGURE 5. Antenna geometry: (a) ground with sequentially rotated slots, (b) feeding network.

energy from the feed network to the radiating patch. The narrowing towards the center concentrates electromagnetic fields, enhancing coupling efficiency. Moreover, this shape enables precise control over field distribution within the antenna, minimizing back radiation and maximizing forward radiation. By adjusting slot dimensions, impedance matching between the feed network and patch is improved, minimizing reflection losses and maximizing power transfer efficiency [8]. The sequential feeding network is illustrated in Fig. 5(b), featuring a progressive 90° phase difference. Specifically, the ports feeding the four coupling slots have phases of 0°, 90°, 180°, and 270° with nearly equal amplitudes. The length of the feed line is optimized to cancel its reactance with respect to the slot aperture. The dimensions of the antenna are provided in Table 1.

The E-field distribution is analyzed across four different frequency bands to determine the polarization type—whether left-handed or right-handed. As depicted in Figure 6, it is evident that the E-field propagates in a clockwise direction, indicating left-handed circular polarization. It is worth noting that by inverting the feed network (feed phases given as 0°, −90°, −180°, −270°) while keeping the rest of the antenna configuration unchanged, right-hand circular polarization (RHCP) can be easily realized. Therefore, the proposed sequentially rotated circularly polarized antenna offers a convenient method for generating both LHCP and RHCP, making it highly promising for wireless communication applications.

TABLE 1. Antenna dimensions (in mm).

Parameter	Value	Parameter	Value
w_1	2.6	w_b	1.5
l_1	24	l_b	17
w_2	4.2	w_c	1.5
l_2	27.3	l_c	24
w_3	6.5	w_d	1.5
l_3	24.3	l_d	24
w_4	6.5	W_G	150
l_4	42	α	45°
w_5	4.2	d_1	48.5
l_5	42	d_2	18
w_6	1.5	d_3	20
l_6	41.4	d_4	20
Wp	115	d_5	2
w_a	1.5	Hs	0.8
l_a	19.9	Hp	15

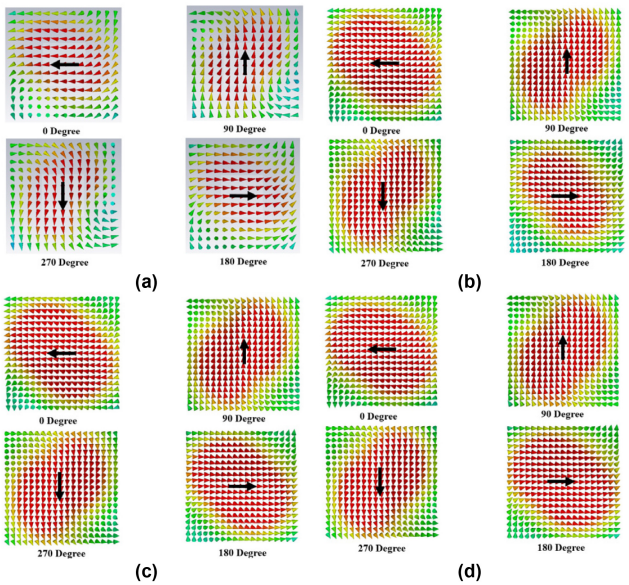

FIGURE 6. E-field distribution at (a) 880 MHz (b) 900 MHz (c) 920 MHz, and (d) 940 MHz validating the generation of CP through a single square patch radiator.

III. RESULTS AND DISCUSSION

The correlation between the results (simulated and experimental) for the proposed sequentially rotated CP antenna is established by simulating the antenna in CST software, followed by fabricating the antenna using an in-house MITS PCB prototyping machine. The multilayer fabricated CP antenna, as illustrated in Fig. 7, occupies a total size of $150 \times 150 \times 15.8\ mm^3$ ($0.42\lambda_\circ \times 0.42\lambda_\circ \times 0.04\lambda_\circ$) at 845 MHz. The antenna's multilayers are stacked together using Teflon rods. The final antenna prototype is soldered with a 50-Ω SMA connector at the input port present on the bottom layer for measurement.

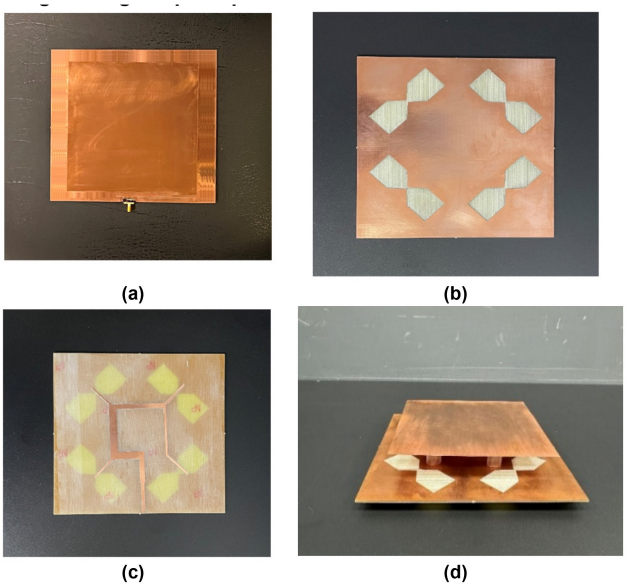

FIGURE 7. Fabricated antenna prototype: (a) top view, (b) top side of bottom layer PCB, (c) bottom side of bottom layer PCB, (d) side view.

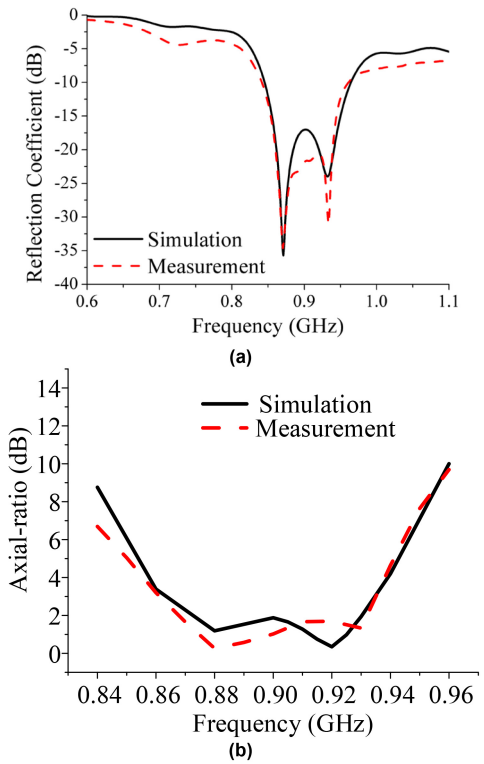

FIGURE 8. Simulated and measured results of (a) reflection coefficient and (b) axial ratio.

The simulated and measured values of the reflection coefficient and axial ratio are depicted in Fig. 8 (a-b) which are obtained using a Keysight N5227B vector network analyzer. The simulated and measured impedance bandwidth ($|S11| \leq -10$ dB) is (13.25%) 845-965 and (13.15%) 845-964, respectively. The simulated antenna illustrates a 3 dB AR BW of (7.80%) 862–932 MHz, while the 3 dB AR BW

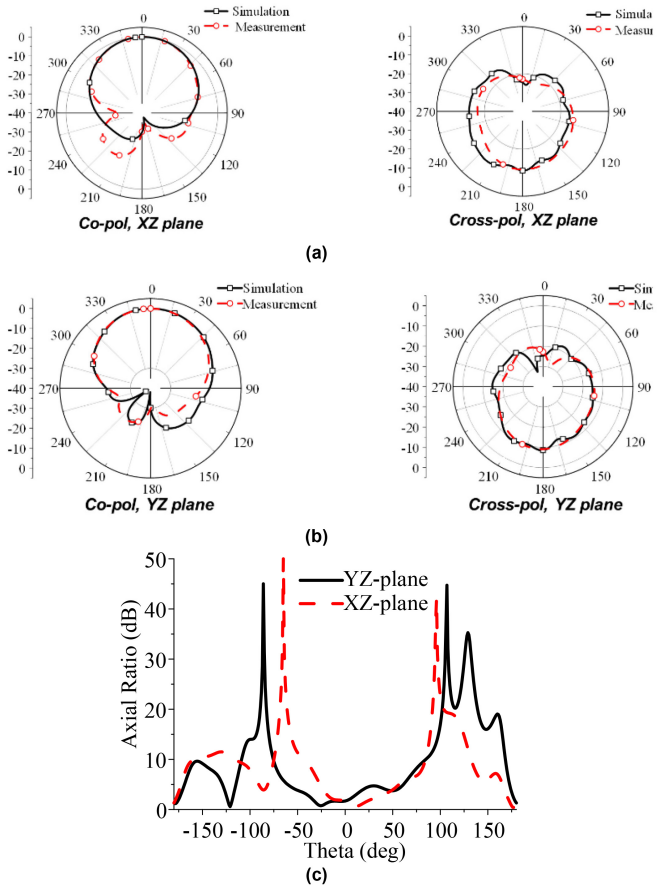

FIGURE 9. Simulated and measured radiation patterns of the sequentially rotated CP antenna at 915 MHz (a) XZ plane (b) YZ plane (c) axial ratio beamwidth.

for the fabricated antenna is (7.45%) 865-932 MHz, showing a strong correlation.

The radiation pattern along xz and yz planes at a center frequency of 915 MHz is simulated and measured. It is illustrated in Fig. 9 (a-b) that the proposed CP antenna provides wide HPBW, a steady directional pattern, and a front-to-back ratio of 8 dB over the band of interest. A slight discrepancy is observed which could be due to the feeding cables in the chamber during measurement and fabrication tolerances. Nevertheless, the simulated and measured levels of RHCP polarization are below −15 dB which indicates a decent circular polarization. The measured values of half-power beam-widths (HPBW) are 70° and 79° and 3 dB AR beam-widths are 62° and 59° along xz and yz planes, respectively with a boresight axial ratio of 1.69 as illustrated in Fig. 9(c).

Similarly, the radiation pattern along xz and yz at 902 MHz and 928 MHz is measured as shown in Fig. 10 (a) which illustrates that the patterns are directional with a reasonable front-to-back ratio. The HPBW and the 3dB AR Beam-width are shown in Fig. 10(b). The measured and simulated gains are plotted in Fig. 11, where a gain value of more than 4.8 dBic is observed across the band of interest. The measured boresight gain at 915 MHz is 7.44 dBic. Overall, a reasonable agreement between simulation and

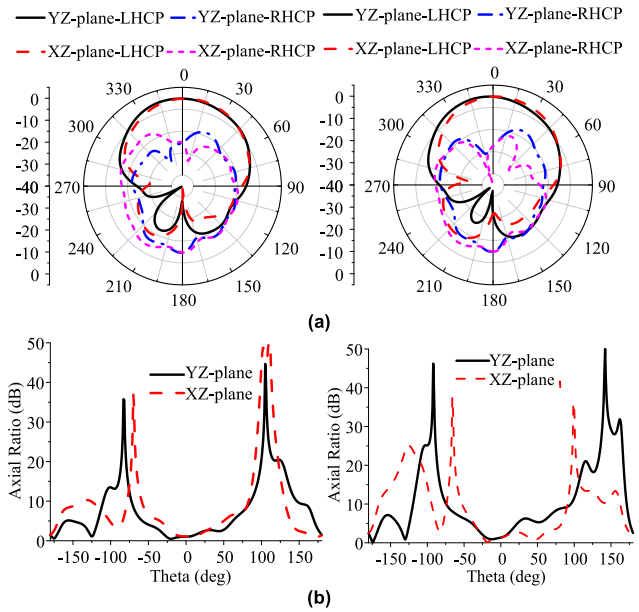

FIGURE 10. Results along XZ- and YZ-planes at 902 MHz (left) and 928 MHz (right) in terms of (a) measured 2D radiation patterns and (b) axial ratio beamwidth.

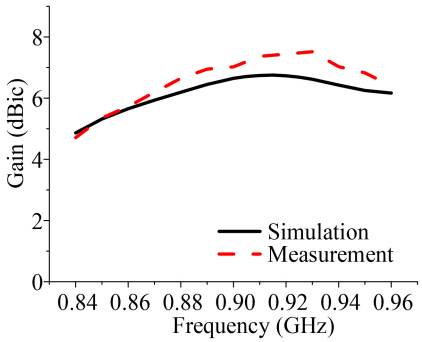

FIGURE 11. Simulated and measured the gain of the proposed antenna.

TABLE 2. Antenna characteristics for chosen parameters.

Frequency (MHz)	Gain (dBic)	AR (dB)	HPBW		3-dB ARBW	
			XZ-plane	YZ-plane	XZ-plane	YZ-plane
902	7.02	1.02	71	80	65	90
915	7.44	1.69	70	79	62	59
928	7.51	1.33	72	74	93	42

measurement was achieved. Table 2 depicts decent values for circular polarization at 902, 915, and 928 MHz, respectively.

To test the CP performance of the proposed antennas, a linearly-polarized tag (ALN 9540) was presented along the boresight direction as depicted in Fig. 12(a). The maximum readable distance was then recorded with the tag rotated at different angles with respect to the line-of-sight direction from the antenna as shown in Fig. 12(b-c). It is evident that at an Effective Isotropic Radiated Power (EIRP) of 2.1W,

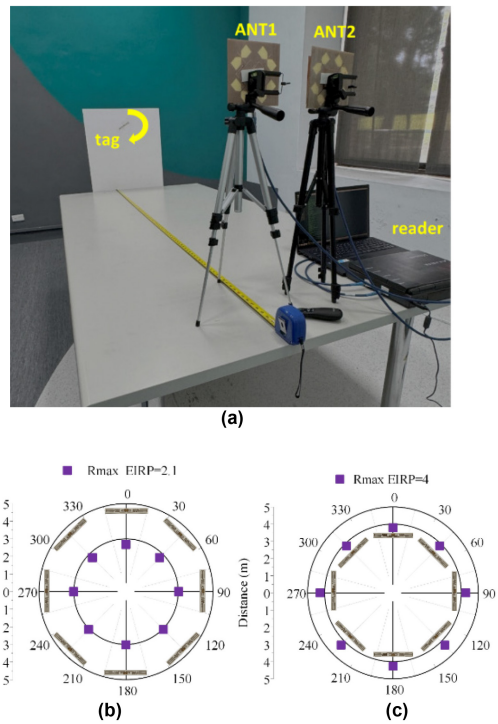

FIGURE 12. RFID antenna read distance measurement: (a) The test setup for tag-reading measurement. The fabricated antenna prototypes (ANT1 and ANT2) are integrated with the ALR-9800 reader. The linearly polarized tag is rotated at different orientations for maximum readable distance measurement. (b) distance for EIRP = 2.1 W; (c) distance for EIRP = 4W.

the maximum readable distance is 2.7 meters, while at an EIRP of 4W, the maximum readable distance is 4 meters. The EIRP is calculated referring to equation (1).

$$\text{EIRP} = \text{Reader output power} + \text{antenna gain} - \text{Cable Loss} \quad (1)$$

The EIRP of 2W (outdoor) and 4W (indoor) is chosen for testing, as that is the permissible limit suggested by the Federal Communications Commission (FCC). The results also demonstrate the good circular polarization (CP) characteristics of the proposed antenna.

In Table 3, comparisons of the proposed antenna are conducted with other state-of-the-art circularly polarized (CP) RFID antennas. In [9], [10], RFID antennas with a low profile are proposed; however, both antennas suffer from low impedance bandwidth (IBW), axial ratio (AR), and gain values, which are less than 3%, 1.64%, and 4 dBic, respectively. A low-profile 2-element RFID antenna with wide IBW (16.4%) is proposed in [11], but it has a low AR bandwidth (4.4%) and gain (4.5 dBic). In [12], a high-gain (18.8 dBic) antenna with an IBW of 10.6% is illustrated, but the antenna has a very large profile ($220 \times 220 \times 11$ mm^3) with a low AR bandwidth (6%). A single-fed antenna with a profile of $150 \times 150 \times 25$ mm^3, having satisfactory IBW and AR bandwidth, is proposed in [13]; however, the gain and overall volume of the antenna may not be suitable for

TABLE 3. Comparison with state-of-the-art CP RFID antennas.

Ref	Size in terms of mm³ (in terms of Lambda at lowest frequency)	No. of elements	IBW (%) Frequency (MHz)	AR BW (%) Frequency (MHz)	F/B Ratio (dB)	Gain (dBic)	AR Beamwidth (Degree)
[9]	60 × 60 × 16.6 ($0.18\lambda_0 \times 0.18\lambda_0 \times 0.05\lambda_0$)	1	(3.0) 909–937	(1.3) 917–929	18	4	--
[10]	45 × 45 × 9 ($0.13\lambda_0 \times 0.13\lambda_0 \times 0.027\lambda_0$)	four meandered monopole elements	(1.63) 912–927	(1.64) 906–921	10	2.2	146
[11]	70 × 70 × 15 ($0.189\lambda_0 \times 0.189\lambda_0 \times 0.04\lambda_0$)	two shorted inverted-L radiating elements	(16.4) 810–960	(4.4) 890–930	--	4.5	--
[12]	220 × 220 × 11 ($0.638\lambda_0 \times 0.638\lambda_0 \times 0.031\lambda_0$)	1 circular patch	(10.6) 870–967	(6) 893–948	16.5	8.9 dBi	--
[13]	150×150×25 ($0.41\lambda_0 \times 0.41\lambda_0 \times 0.069\lambda_0$)	half E-shaped patch, a near-field resonant parasitic (NFRP) patch	(14.2) 833-960	(9.0) 846-926	15	7.3	--
[14]	60 × 60 × 15 ($0.168\lambda_0 \times 0.168\lambda_0 \times 0.042\lambda_0$)	4	(13.3) 840-960	(13.3) 840-960	--	2.2	--
[15]	95×100×13.6 ($0.23\lambda_0 \times 0.249\lambda_0 \times 0.033\lambda_0$)	four sequentially rotated inverted-F antennas	(36.0) 748 - 1.076 GHz	(18.6) 805- 970	--	3.1	--
[16]	150×150×21 ($0.365\lambda_0 \times 0.365\lambda_0 \times 0.051\lambda_0$)	Square ring-shaped patch	(30.2) 730–990	(24.2) 760–970	13	5.6	--
[17]*	105×54×9.6 ($1.64\lambda_0 \times 0.84\lambda_0 \times 0.15\lambda_0$)	4	(30.9) 4.7-6.4	(23.52) 4.5-5.7	--	10	--
[18]*	36×36×5.74 ($1.02\lambda_0 \times 1.02\lambda_0 \times 0.16\lambda_0$)	4	(40) 8-12	(37) 8.5-12.3	--	10.3	--
This work	150×150×15.8 ($0.42\lambda_0 \times 0.42\lambda_0 \times 0.04\lambda_0$)	1	(13.15) 845-964	(7.45) 865-932	8	7.8	105

*DRA Based antenna; IBW: Impedance bandwidth; AR: Axial ratio; F/B: Front to back

many applications. In [14], an antenna with decent IBW and AR bandwidth and a low profile is proposed, although the antenna displays a very low gain of only around 2.2 dBic. An antenna with high IBW (36%) and AR bandwidth (18.6%) with a profile of 95 × 100 × 13.6 mm^3 is depicted in [15]; however, this antenna also suffers from low gain (3.1 dBic). In [16], an antenna with a size of 150 × 150 × 21 mm^3 is illustrated, achieving a very wide IBW (30.2%) and AR bandwidth (24.2%); however, the overall volume and gain (5.6 dBic) limit its use for specific RFID applications. As observed, although the antennas in [17], [18] offer wider IBW and AR BW, the overall size is large in terms of the operating wavelength. Moreover, DRA's generally require high precision in terms of manufacturing and positioning. Out of the RFID antennas discussed, only [10] is analyzed for both front-to-back ratio and AR beam width.

The proposed CP antenna features left-hand circularly-polarized (LHCP) radiation characteristics with a gain of 7.8 dBic, a front-to-back (F/B) ratio of 8 dB, AR beamwidth of more than 105°, IBW of (13.15%) 845-964 MHz, and an AR bandwidth (AR<3 dB) of (7.45%) 865-932 MHz. The read range of the reader antenna is 2.7 meters and 4 meters at an effective isotropic radiated power (EIRP) of 2.1 W and 4 W, respectively. The use of sequential rotational feed with inclined slot geometry helps in achieving enhanced AR beam width and bandwidth with only a single radiator at the top.

IV. CONCLUSION

In this paper, a technique for circular polarization (CP) generation using a single radiator has been proposed. Leveraging the operational mechanisms of conventional sequentially-rotated radiator antennas, the implementation of a sequentially-rotated feeding network enabled similar CP performance while maintaining size compactness. The technique was validated using a commercial radio-frequency identification (RFID) system at the 915 MHz band, where the antenna exhibited satisfactory CP performance. The proposed technique is a generic approach suitable for any type of feeding excitation, including coupling through slots or pins.

ACKNOWLEDGMENT

The authors would like to thank Dr. Ting-Jui Huang for valuable discussions on the design of the antenna.

REFERENCES

[1] S. M. A. M. Hasan Abadi and N. Behdad, "Wideband linear-to-circular polarization converters based on miniaturized-element frequency selective surfaces," *IEEE Trans. Antennas Propag.*, vol. 64, no. 2, pp. 525–534, Feb. 2016.

[2] I. Nadeem et al., "A comprehensive survey on 'circular polarized antennas' for existing and emerging wireless communication technologies," *J. Phys. D, Appl. Phys.*, vol. 55, no. 3, Oct. 2021, Art. no. 33002.

[3] J.-D. Zhang, L. Zhu, N.-W. Liu, and W. Wu, "Dual-band and dual-circularly polarized single-layer microstrip array based on multiresonant modes," *IEEE Trans. Antennas Propag.*, vol. 65, no. 3, pp. 1428–1433, Mar. 2017.

[4] R. F. Harrington, "Effect of antenna size on gain, bandwidth, and efficiency," *J. Res. Natl. Bureau Stand. D. Radio Propag.*, vol. 64, no. 1, p. 1, Jun. 1959.

[5] M. Fairouz and M. A. Saed, "A sequentially rotated, circularly polarized microstrip antenna array with reduced mutual coupling," *Electromagnetics*, vol. 36, no. 7, pp. 422–433, Sep. 2016.

[6] S. Fu, Q. Kong, S. Fang, and Z. Wang, "Broadband circularly polarized microstrip antenna with coplanar parasitic ring slot patch for L-band satellite system application," *IEEE Antennas Wireless Propag. Lett.*, vol. 13, pp. 943–946, 2014.

[7] J. Huang, "A technique for an array to generate circular polarization with linearly polarized elements," *IEEE Trans. Antennas Propag.*, vol. 34, no. 9, pp. 1113–1124, Sep. 1986.
[8] G. Kumar and K. P. Ray, *Broadband Microstrip Antennas*. Boston, MA, USA: Artech House, 2003.
[9] Y.-F. Lin, C.-H. Lee, S.-C. Pan, and H.-M. Chen, "Proximity-fed circularly polarized slotted patch antenna for RFID handheld reader," *IEEE Trans. Antennas Propag.*, vol. 61, no. 10, pp. 5283–5286, Oct. 2013.
[10] J.-H. Bang, C. Bat-Ochir, H.-S. Koh, E.-J. Cha, and B.-C. Ahn, "A small and lightweight antenna for handheld RFID reader applications," *IEEE Antennas Wireless Propag. Lett.*, vol. 11, pp. 1076–1079, 2012.
[11] Y.-F. Lin, H.-M. Chen, C.-H. Chen, and C.-H. Lee, "Compact shorted inverted-L antenna with circular polarisation for RFID handheld reader," *Electron. Lett.*, vol. 49, no. 7, pp. 442–444, Mar. 2013.
[12] X. Chen, G. Fu, S.-X. Gong, Y.-L. Yan, and W. Zhao, "Circularly polarized stacked annular-ring microstrip antenna with integrated feeding network for UHF RFID readers," *IEEE Antennas Wireless Propag. Lett.*, vol. 9, pp. 542–545, 2010.
[13] J. Li, H. Liu, S. Zhang, M. Luo, Y. Zhang, and S. He, "A wideband single-fed, circularly-polarized patch antenna with enhanced axial ratio bandwidth for UHF RFID reader applications," *IEEE Access*, vol. 6, pp. 55883–55892, 2018.
[14] L. Zhu et al., "Compact wideband circularly-polarized antenna for universal UHF RFID handheld reader," *Microw. Opt. Technol. Lett.*, vol. 63, no. 4, pp. 1201–1206, Apr. 2021.
[15] Q. Liu, J. Shen, H. Liu, Y. Wu, M. Su, and Y. Liu, "Low-cost compact circularly polarized directional antenna for universal UHF RFID handheld reader applications," *IEEE Antennas Wireless Propag. Lett.*, vol. 14, pp. 1326–1329, 2015.
[16] J. Li, H. Liu, S. Zhang, Y. Zhang, and S. He, "Compact broadband circularly-polarized antenna with a backed cavity for UHF RFID applications," *IET Microw. Antennas Propag.*, vol. 13, no. 6, pp. 789–795, Mar. 2019.
[17] S. Gupta, A. Sharma, G. Das, R. K. Gangwar, and M. Khalily, "Wideband circularly polarized dielectric resonator antenna array with polarization diversity," *IEEE Access*, vol. 7, pp. 49069–49076, 2019.
[18] M. S. Ibrahim, H. Attia, Q. Cheng, and A. Mahmoud, "Wideband circularly polarized aperture coupled DRA array with sequential-phase feed at X-band," *Alexandria Eng. J.*, vol. 59, no. 6, pp. 4901–4908, 2020.

HENG-TUNG HSU (Senior Member, IEEE) received the B.S. and M.S. degrees in electronics engineering from the National Chiao Tung University, Hsinchu, Taiwan, in 1993 and 1995, respectively, and the Ph.D. degree in electrical and computer engineering from the University of Maryland at College Park, College Park, MD, USA, in 2002.

Since 2015, he has been with the International College of Semiconductor Technology, National Yang Ming Chiao Tung University, where he is currently a Professor. He has authored or coauthored more than 100 journal papers and holds three U.S. patents. His research interest includes the design and implementation of RF front-ends, antennas, active and passive microwave components, and RF packaging.

YI-FAN TSAO (Member, IEEE) received the B.S. degree in electro-physics from National Chiao Tung University, Hsinchu, Taiwan, in 2016, the M.S. degree in electrical engineering from the University of California at Los Angeles, Los Angeles, USA, in 2018, and the Ph.D. degree in electrical and computer engineering from Technische Üniversität Berlin, Berlin, Germany in 2022. He worked as a Ph.D. Research Fellow with the GaN Power Electronics and Microwave Devices Lab, Ferdinand Braun Institute, Berlin, Germany, from 2019 to 2022. He is currently working as an Assistant Professor with the Industry Academia Innovation School, Institute of Pioneer Semiconductor Innovation, National Yang Ming Chiao Tung University. His research interests include design of millimeter-wave front-end circuits, development of RF transceiver modules, and reliability assessment of III–V compound semiconductor devices.

ARPAN DESAI (Senior Member, IEEE) received the B.E. degree in electronics and communication engineering from Sardar Patel University, India, in 2006, the M.Sc. degree in wireless communication systems from Brunel University, London, U.K., in 2008, and the Ph.D. degree from the Charotar University of Science and Technology, India, in January 2020. He is currently working as an Assistant Professor with Pandit Deendayal Energy University, Gandhinagar, India. Previously he was engaged as a Research Scientist with the mm-wave Lab, International College of Semiconductor Technology, National Yang-Ming Chiao Tung University, Taiwan. Prior to this, he held the position of Assistant Professor with the Electronics and Communication Engineering Department, Charotar University of Science and Technology, India. He also served as a Postdoctoral Fellow with Ton Duc Thang University, Ho Chi Minh, Vietnam, specializing in RF and Microwave technology. He has contributed over 80 research articles in peer-reviewed journals, conferences, and book chapters. His exceptional contributions to the field of antenna design and his extensive research output underscore his standing in the top 2% of scientists worldwide based on the list curated by Stanford University. His current research pursuits encompass a range of topics, including mm-wave antennas, transparent antennas, MIMO antennas, circularly polarized antennas, and flexible antennas. He is the Vice Chair for the IEEE Signal Processing Society, Gujarat Section, India, and serves as an associate editor of a few referred journals. Additionally, he serves as a reviewer for numerous reputable journals.